

Casein kinase 1 inhibitor avoids TDP-43 pathology propagation in a patient-derived cellular model of amyotrophic lateral sclerosis

Eva P. Cuevas^{a,b,1}, Loreto Martinez-Gonzalez^{a,b,1}, Clara Gordillo^a, Carlota Tosat-Bitrián^{a,b}, Carmen Pérez de la Lastra^c, Amets Sáenz^{b,d}, Carmen Gil^a, Valle Palomo^{b,c}, Ángeles Martín-Requero^{a,b}, Ana Martínez^{a,b,*}

^a Centro de Investigaciones Biológicas “Margarita Salas”-CSIC, Ramiro de Maeztu 9, 28040 Madrid, Spain

^b Centro de Investigación Biomédica en Red en Enfermedades Neurodegenerativas, (CIBERNED), Instituto de Salud Carlos III, Av. Monforte de Lemos, 3-5, 28029 Madrid, Spain

^c Instituto Madrileño de Estudios Avanzados en Nanociencia (IMDEA-Nanociencia), C/Faraday 9, Cantoblanco, 28049 Madrid, Spain

^d Biodonostia Health Research Institute, Neurosciences Area, 20014 San Sebastian, Spain

ARTICLE INFO

Keywords:

Amyotrophic lateral sclerosis
TDP-43
CK-1 inhibitor
Benzothiazole IGS2.17
Cell-to-cell disease propagation, extracellular vesicles

ABSTRACT

Amyotrophic lateral sclerosis is a fatal neurodegenerative disease without a cure to reverse its progression. Its main hallmark is the nuclear protein TDP-43, which undergoes different post-translational modifications leading to a loss of function in the nucleus and an increase in toxicity in the cytoplasm. Previous reports have indicated that pathogenic TDP-43 exhibits prion-like propagation in various contexts. With the aim of advancing therapeutics focused on preventing the propagation of TDP-43 pathology, we studied the potential role of pathogenic TDP-43 in lymphoblasts from sporadic ALS patients. We used lymphoblastoid cell lines from sporadic ALS patients as a source of pathogenic forms of TDP-43, and healthy human cells (lymphoblasts, myoblasts, neuroblastoma SH-SY5Y, or osteosarcoma U2OS) as recipient cells to investigate the seeding and spread of TDP-43 proteinopathy. Furthermore, we evaluated the potential of targeting TDP-43 phosphorylation with a CK-1 inhibitor to prevent the propagation of the pathology. The results presented herein indicate that pathogenic forms of TDP-43 are secreted into the extracellular medium of sporadic ALS lymphoblasts and could be transported by extracellular vesicles, spreading TDP-43 pathology to healthy cells. Moreover, tunneling nanotubes have also been discovered in pathological cells and may be involved in the transport of TDP-43. Interestingly, targeting TDP-43 phosphorylation with an in-house designed CK-1 inhibitor (IGS2.7) was sufficient to halt TDP-43 pathology transmission, in addition to its known effects on restoring the homeostasis of TDP-43 protein in patient-derived cells.

List of abbreviations

ALS	amyotrophic lateral sclerosis
BBB	blood–brain barrier
CK-1	casein kinase 1
CM	conditioned medium
EV	extracellular vesicles
FBS	fetal bovine serum
TDP-43	transactive response DNA-binding protein of 43 KDa
TNT	tunneling nanotubes

1. Introduction

Amyotrophic lateral sclerosis (ALS) is an adult-onset, rapidly progressive disorder characterized by selective degeneration of upper and lower motor neurons, leading to the loss of control of voluntary muscle movement. The disease may initially manifest focally in a single limb but then progressively spreads segmentally through the spinal cord and the motor cortex until respiratory muscles fail (Masrori and Van Damme, 2020).

ALS has no cure, and there is no effective treatment to reverse its progression. To date, only a limited number of therapies are approved

* Corresponding author at: Centro de Investigaciones Biológicas “Margarita Salas”-CSIC, Ramiro de Maeztu 9, 28040 Madrid, Spain.

E-mail address: ana.martinez@csic.es (A. Martínez).

¹ These authors contributed equally to this work.

<https://doi.org/10.1016/j.nbd.2024.106430>

Received 26 November 2023; Received in revised form 2 February 2024; Accepted 4 February 2024

Available online 5 February 2024

0969-9961/© 2024 The Authors. Published by Elsevier Inc. This is an open access article under the CC BY license (<http://creativecommons.org/licenses/by/4.0/>).

for sporadic ALS, including riluzole, edaravone, and, very recently sodium phenylbutyrate/taurursodiol. However, these drugs only offer modest clinical benefits in disease progression and are available in only a few countries (Tzeplaeff et al., 2023). Life expectancy after diagnosis is typically 2–5 years, making the search for more suitable treatments an urgent need to slow the disease progression and extend the lifespan of ALS patients.

Transactive response DNA-binding protein of 43 kDa (TDP-43) becomes ubiquitinated and hyper-phosphorylated, forming cytosolic aggregates that are considered the primary hallmark of ALS. TDP-43 aggregates contain full-length 43 kDa protein as well as C-terminal fragments of 35 and 25 kDa, which exhibit differential seeding properties and toxicity (Berning and Walker, 2019). This pathological phenomenon is present in the majority of all ALS patients, regardless of the mechanism of disease onset (Neumann et al., 2006).

TDP-43 pathology in ALS may disseminate in a sequential pattern that allows for recognition of four neuropathological disease stages (Brettschneider et al., 2013). In stage I, phosphorylated (p-TDP-43) inclusions are observed in motor neurons of the cortex, brainstem, and spinal cord, while in the final stage, p-TDP-43 inclusions progress to reach the temporal lobe or the hippocampus (Braak et al., 2013). These clinical features suggest cell-to-cell disease dissemination.

Previous reports indicate that pathogenic TDP-43 exhibits prion-like propagation in murine brain and spinal cord of TDP-43 transgenic animals treated with ALS patient-derived cerebrospinal fluid (Mishra et al., 2020). Additionally, spinal cord extracts from sporadic ALS patients spread TDP-43 pathology to cerebral organoids (Tamaki et al., 2023). However, the mechanism by which this occurs is not yet well understood.

This study aimed to gain insight into the potential role of pathogenic TDP-43 derived from immortalized lymphocytes of sporadic ALS (sALS) patients in healthy cells, with the goal of advancing therapeutics focused on preventing the propagation of TDP-43 pathology. To achieve this, we utilized lymphoblastoid cell lines from sALS patients as a source of pathogenic forms of TDP-43, and healthy cells (including lymphoblasts, myoblasts or human neuroblastoma or osteosarcoma cell lines, SH-SY5Y and U2OS, respectively) as recipient cells to investigate the seeding and spread of the TDP-43 proteinopathy. Additionally, we evaluated the potential of targeting TDP-43 phosphorylation to prevent the propagation of the pathology, as this event appears to play a key role in these processes (Porta et al., 2018). To do so, we employed a small heterocycle molecule prepared in our laboratory, which is a potent and selective casein kinase 1 (CK1) inhibitor.

We previously reported that lymphoblasts from sALS patients exhibit pathological TDP-43 features (Posa et al., 2019). The suitability of these lymphoblastoid cell lines as a pharmacological platform to test potential disease-modifying drugs has been extensively demonstrated (Vaca et al., 2021; Martínez-González et al., 2021; Nozal et al., 2022). The results presented here indicate that pathogenic forms of TDP-43 are present in the extracellular medium and may promote the spread of TDP-43 pathology to healthy cells. Moreover, tunneling nanotubes (TNT)-like structures have been discovered in patient-derived cells and may be involved in the transport of TDP-43 between cells. Interestingly, targeting TDP-43 phosphorylation with an in-house-designed benzothiazole-based CK-1 inhibitor, namely IGS2.7, was sufficient to halt the dissemination of TDP-43 pathology, in addition to its known effects on restoring phosphorylation levels and mislocalization of TDP-43 protein in patients-derived cells.

2. Materials and methods

2.1. Materials

DMEM culture medium (Cat#41965039, Gibco/Thermo Fisher, Waltham, MA, USA), RPMI 1640 culture medium (Cat#21875034, Gibco/Thermo Fisher, Waltham, MA, USA), Lonza BioWhittaker

Medium 199 (M-199) with Earle's BSS (Cat#BE12-117F, Thermo Fisher, Waltham, MA, USA), Foetal Bovine Serum (FBS) (Cat#: F7524 Merck, Madrid, Spain), Exosome-depleted FBS (Cat#: A2720801, Gibco, Waltham, MA, USA), penicillin/ streptomycin (Cat#15140-122, Gibco/Thermo Fisher Waltham, MA, USA), fungizone (Cat#15290-018, Gibco/Thermo Fisher, Waltham, MA, USA), human recombinant insulin (Cat#T2643-50, Sigma-Aldrich, Carlsbad, CA, USA), L-glutamine 200 mM (Cat#25030-32, Gibco/Thermo Fisher, Waltham, MA, USA), human Epidermal Growth Factor (hEGF) (Cat#AF-100-15, Peprotech/Thermo Fisher, Waltham, MA, USA), Fibroblasts Growth Factor (FGF) (Cat#100-18-B, Peprotech/Thermo Fisher, Waltham, MA, USA), polyvinylidene difluoride (PVDF) membranes for Western blots (Bio-Rad, Alcobendas, Madrid, Spain), enhanced chemiluminescence (ECL) system (Amersham, Uppsala, Sweden), protease inhibitor complete mini mixture (Roche, Mannheim, Germany), Pierce BCA Protein Assay kit (Thermo Fisher, Waltham, MA, USA).

The CK-1 protein inhibitor, benzothiazole derivative IGS2.7, was synthesized in our laboratory following previously described procedures (Salado et al., 2014). The chemical structure, IC₅₀ value for kinase inhibition, as well as the effective permeability value predicting its ability to cross the blood–brain barrier (BBB), along with some *in vivo* pharmacokinetics parameters, are provided in Table 1.

Antibodies used in this study and supplier companies are listed in Table 2.

2.2. Subjects

Blood samples were obtained from eight sALS patients and five age-matched control subjects after obtaining written informed consent. All patients were diagnosed using the revised El Escorial criteria (Brooks et al., 2000) at the Hospital Doce de Octubre (Madrid, Spain). All procedures were conducted in accordance with National and European Union Guidelines and approved by the Institutional Review Board of Hospitals Doce de Octubre (CEICO2506) and the Ethics Committee of the Spanish Council of Higher Research (protocol code B2017/BMD-3813, dated 1 February 2018). Demographic and clinical information of control subjects and ALS patients are presented in Table 3.

2.3. Establishment of lymphoblastoid cell lines

Peripheral blood mononuclear cells (PBMCs) were isolated from blood samples by Lymphoprep™ density-gradient centrifugation following the manufacturer's instructions (Axis-Shield Po CAS, Oslo, Norway). Lymphoblastoid cell lines were established in our laboratory by infecting peripheral blood lymphocytes with the Epstein–Barr virus, as previously described (Hussain and Mulherkar, 2012).

2.4. Cell culture

Lymphoblastoid cell lines (LCLs) were cultured in suspension in RPMI 1640 medium (1×10^6 cells/mL) supplemented with 1% penicillin/ streptomycin and 10% (v/v) fetal bovine serum (FBS) in upright T flasks. LCLs were used individually, and experiments were not conducted in a blinded manner. The neuroblastoma SH-SY5Y cell line and U2OS cells (obtained from the American Type Culture Collection) were cultured in DMEM media containing 10% (v/v) FBS and 1% penicillin/ streptomycin.

Myoblasts were obtained from healthy individuals who underwent surgery for bone fractures, and the muscle biopsies were collected during the surgical procedure. In all cases, participants provided informed consent using forms approved by the Ethics Committee on the Use of Human Subjects in Research at Donostia University Hospital. Human proximal muscle biopsies were minced and cultured in a monolayer according to the method described by Askanas (Askanas and Engel, 1975). To obtain highly purified myoblasts (CD56+) and (CD56-) cells, primary cultures were sorted by immunomagnetic selection based on the

Table 1Chemical structure, IC₅₀ value of CK-1 inhibition, BBB penetration prediction and pharmacokinetic *in vivo* parameters of IGS2.7.

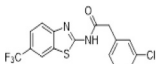
Comp.	Chemical structure	CK-16 IC ₅₀	BBB prediction	Pe (10 ⁻⁶ cm.s ⁻¹)	C _{max} Plasma (ng.ml ⁻¹) (15) i.p. p.o.	C _{max} Brain (ng.g ⁻¹) (15) i.p. p.o.
IGS2.7		23 ± 2 nM	CNS +	11.3 ± 2.0	224.511120.42	670.563940.51

Table 2

Antibodies used in this study.

Primary Antibody	Species	Dilution (WB/IF)	Supplier (Catalog#)
TDP-43	Rabbit	1:1000/NA	Proteintech (10782-2-AP)
TDP-43	Mouse	1:1000/1:100	Proteintech (67345-1-Ig)
p(Ser409/410)-TDP-43	Rabbit	1:500/1:1000	Proteintech (22309-1-AP)
α-Tubulin	Mouse	1:5000/NA	Santa Cruz (23948)
GAPDH	Rabbit	1:1000/NA	Cell Signal (5174)
Flotillin-1	Rabbit	1:1000/NA	Thermo Fisher (PA5-97756)
Kinesin 1 (KIF5B)	Rabbit	NA/1:100	Proteintech (21632-1-AP)

Secondary Antibody	Immunological Procedure	Dilution	Supplier (Catalog#)
Goat anti-mouse IgG HRP conjugate	WB	1:7000	Bio-Rad (1706516)
Goat anti-rabbit IgG HRP conjugate	WB	1:7000	Bio-Rad (1706516)
anti-mouse Alexa 488	IF	1:1000	Molecular Probes (A-11001)
anti-mouse Alexa 568	IF	1:1000	Molecular Probes (A-11004)
Dylight 488 horse anti-rabbit	IF	1:1000	Vector

WB:Western blot; IF:immunofluorescence; NA:not applicable.

Table 3

Demographic and clinical characteristics of participants.

Code	Gender	Age at sample obtention	Clinical presentation	Motor neuron affected
C100	Female	83	NA	NA
C110	Male	75	NA	NA
C105	Female	54	NA	NA
C106	Female	67	NA	NA
C108	Female	68	NA	NA
E2	Female	76	bulbar	MNS
E4	Female	53	bulbar	MNS + MNI
E6	Female	79	bulbar	MNI
E10	Male	68	bulbar	NK
ED5	Female	82	bulbar & spinal	NK
ED8	Female	59	spinal	MNI
ED10	Male	67	spinal	NK
ED11	Female	65	NK	MNS + MNI

NA: not applicable; MNS, MNI: superior and inferior motor neuron, respectively; NK: Not known.

presence of the early cell surface marker CD56 (separator and reagents from Miltenyi Biotec). CD56⁺ cells were seeded at 2500–3000 cells/cm² in culture medium for the myoblast stage. Myoblasts were then grown in DMEM media supplemented with 20% M-199, 10% FBS, 1% penicillin/streptomycin/fungizone, 1% insulin, 1% glutamine, 0.1% hEGF and 0.5% FGF. Before seeding cells, plates were coated with 0.1% gelatine for 1 h. All cell lines were grown at 37 °C in a humidified 5% CO₂ atmosphere.

The experimental outline followed is summarized in [Scheme 1](#).

2.5. Extracellular vesicles isolation and characterization

RPMI medium containing 10% exosome-depleted FBS was used to culture lymphoblasts to generate conditioned medium for extracellular vesicles (EVs) isolation. After 72 h, cells and debris were removed from the conditioned media by centrifuging it at 2000 ×g for 30 min. EVs were isolated with total exosome isolation reagent (Invitrogen) following manufacturer's recommendations. 1.5 mL of the reagent was added to 3 mL of the conditioned media, and it was incubated overnight at 4 °C. The following day, samples were centrifuged at 10,000 g for 1 h at 4 °C. The supernatant was discarded, and the pellet containing EVs was suspended in 30 μL of Phosphate-Buffer Saline (PBS) for characterization or for further use in the treatment of healthy control lymphoblastoid cells.

EV characterization was conducted using nanoparticle tracking analysis (NTA) and Western Blot. Size distribution and quantification of EVs preparations were examined by measuring the rate of Brownian motion with a NanoSight NS300 system equipped with a 488 nm laser, fast video capture, and particle-tracking software. PBS was used to dilute EVs samples (1:9000), which were disaggregated before being injected into the NanoSight's sample chamber. The mean number of particles acquired per milliliter in ALS and control cells was compared, and EV concentration measurements (particles/mL) were normalized to the cell number from which conditioned medium containing EVs was recollected. For Western Blot (WB) analysis 20 μL of EVs were lysed with Laemmle buffer and denatured at 95 °C for 5 min. The antibodies used are listed in [Table 2](#).

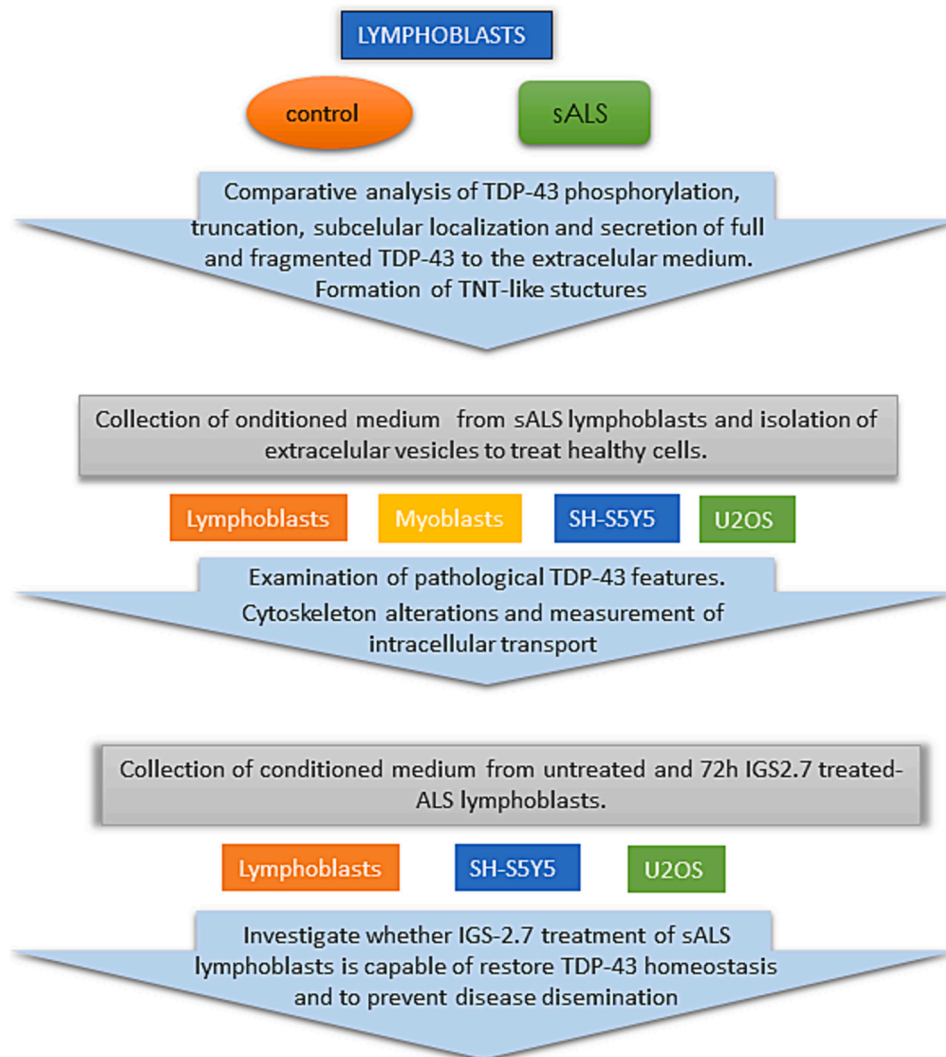
2.6. Conditioned medium experiments

ALS lymphoblasts were treated with or without IGS2.7 (5 μM). This dose of IGS2.7 was sufficient to restore TDP-43 homeostasis in diseased cells. Conditioned medium (CM) or pre-treated CM (ptCM) were collected after 72–96 h and added to healthy cells (including healthy lymphoblasts, U2OS, myoblasts, SH-SY5Y) in a ratio 3:1 with fresh medium as previously described ([Cuevas et al., 2022](#)). Cells were harvested 72 h later and processed for Western blot and/or immunofluorescence analysis.

2.7. Western blot analysis

For extracellular TDP-43 analysis, ALS and healthy lymphoblast were grown, and the conditioned medium was collected after 72 h. To prepare cell extracts for WB analysis, cells were harvested by centrifugation, washed in PBS, and then lysed in ice-cold lysis buffer (50 mM Tris-HCl (pH 7.4), 150 mM NaCl, 5 mM EDTA, 15 mM MgCl₂, 0.5% (vol/vol) sodium deoxycholate, 0.5% (vol/vol) NP-40 and 0.1% (vol/vol) SDS), containing 1 mM sodium orthovanadate, 1 mM phenylmethylsulfonyl fluoride (PMSF), 1 mM sodium pyrophosphate and protease inhibitor mixture. The protein content was quantified using the Pierce BCA Protein Assay kit (Thermo Scientific).

Equal amounts of proteins or 30 μL of medium were resolved by SDS-polyacrylamide gel electrophoresis. The proteins were then transferred to polyvinylidene fluoride (PVDF) membranes, blocked with 5% BSA in TTBS 1×, and immunodetected with the antibodies listed in [Table 2](#). Signals from the primary antibodies (4 °C, overnight) were amplified using species-specific antisera conjugated with horseradish



Scheme 1. Flowchart of experimental design. Subjects listed in Table 3 provided control and ALS lymphoblasts. Additionally, human myoblasts, neuroblastoma SH-SY5Y, and osteosarcoma U2OS cell lines were utilized. IGS2.7, an in-house designed CK-1 inhibitor, was employed in the experiments.

peroxidase (Bio-Rad) and detected with a chemiluminescent substrate detection system ECL using the Chemidoc Imaging System (Bio-Rad, Alcobendas, Madrid, Spain). Image J software (National Institutes of Health, Bethesda, MD, USA) was used to quantify relative band intensities.

2.8. Immunofluorescence analysis

Adherent cells (myoblasts, U2OS and SH-SY5Y) were grown on coverslips. To facilitate the adhesion of lymphoblastoid cells, coverslips were first treated with a solution of 0.25% Gelatin (Sigma, Madrid, Spain) for 30 min at room temperature, followed by a solution of 1 mg/mL poly-L-lysine (Sigma, Madrid, Spain) diluted 1:50 in Borax buffer (Na₂B₄O₇·10H₂O 15 mM, pH 8.4) overnight at 37 °C. Cells were fixed for 30 min in 4% paraformaldehyde in PBS and permeabilized with 0.1% Triton X-100 for 10 min. Samples were then blocked with PBS containing 1% BSA for 60 min at 37 °C before incubation overnight with the primary antibodies (Table 2). After several washes in PBS, samples were incubated with the appropriate secondary antibodies for 1 h at 37 °C. For nuclear and F-actin staining, DAPI (1:1000, Sigma) and Alexa Fluor-568 Phalloidin (1:1000, Molecular Probes, Waltham, MA, USA) were used, respectively. Preparations were mounted with Fluor Save reagent (Calbiochem, Madrid, Spain). High-resolution images were acquired

using a confocal microscope Leica TCS SP5 with 63× or 100× oil immersion objectives. Leica Application Suite X (version 3.5.7.23225) and Image J software (version 1.53 K) were used to analyze images.

2.9. Peptide probes

Peptide tools containing a kinesin binding domain and a cell-penetrating region were synthesized and fluorescently labeled at the N-termini with the organic fluorophore Cy5 to obtain the fluorescent probes Cy5-KBP. Their synthesis, labeling and purification were performed as previously described (Oliva et al., 2022).

2.10. Intracellular transport analysis

U2OS cells were seeded on 8-well ibidi plates and exposed for 72 h to conditioned medium from healthy individuals, sALS lymphoblasts, or lymphoblasts treated with IGS2.7 (5 μM). Subsequently, the medium was removed, and the probe Cy5-KBP was added to the cells at a concentration of 2.5 μM for 15 min at 37 °C. Peptides were washed using DMEM without phenol red. Images were acquired using a confocal laser scanning microscope Leica TCS SP8 with a 63× oil immersion objective equipped with a humidified incubation chamber, a CO₂ controller, and a heating unit. Cy5 fluorescence emission was collected at 660–720 nm

after excitation at 646 nm. Images were recorded every 1.793 s for 4 min as 2-layer-z-stacks. Three different fields for each condition were imaged in two separate experiments.

Analysis of single-particle trajectories was performed using the TrackMate plugin within the ImageJ software. The LoG detector and the linear motion LAP tracker were specifically utilized to detect and link particles, with an estimated blob diameter of 1 μm and a maximum distance of 2 μm . Additional filters were applied to discard trajectories with fewer than 5 spots and with a maximum speed of 1 $\mu\text{m s}^{-1}$. Track mean velocity, track maximal velocity, and track mean displacement were then calculated and normalized to control cells in each experiment.

2.11. Statistical analysis

Graph Pad Prism software version 6 (La Jolla, CA, USA) was used to performed statistical analysis. All data are presented as mean \pm standard error of the mean (SEM). Statistical significance was assessed using a

two-tailed Student's *t*-test for comparisons between two groups, or one-way ANOVA followed by Bonferroni's post-hoc analysis for multiple comparisons. A "p-value < 0.05" was considered statistically significant.

3. Results

3.1. ALS lymphoblasts exhibit TDP-43 post-translational modifications and cytoskeletal abnormalities

We utilized lymphoblasts from sporadic ALS patients as an experimental model, as these cells recapitulate TDP-43 pathology (Posa et al., 2019; Porras et al., 2023). Data presented in Fig. S1, obtained from immortalized lymphocytes of 5 healthy donors and 8 sALS patients, align with previous findings from our laboratory (Posa et al., 2019), demonstrating increased cytosolic TDP-43 phosphorylation. Using phalloidin to stain filamentous actin (F-actin), we observed actin cytoskeleton alterations reminiscent of tunneling nanotubes (TNTs) or TNT-

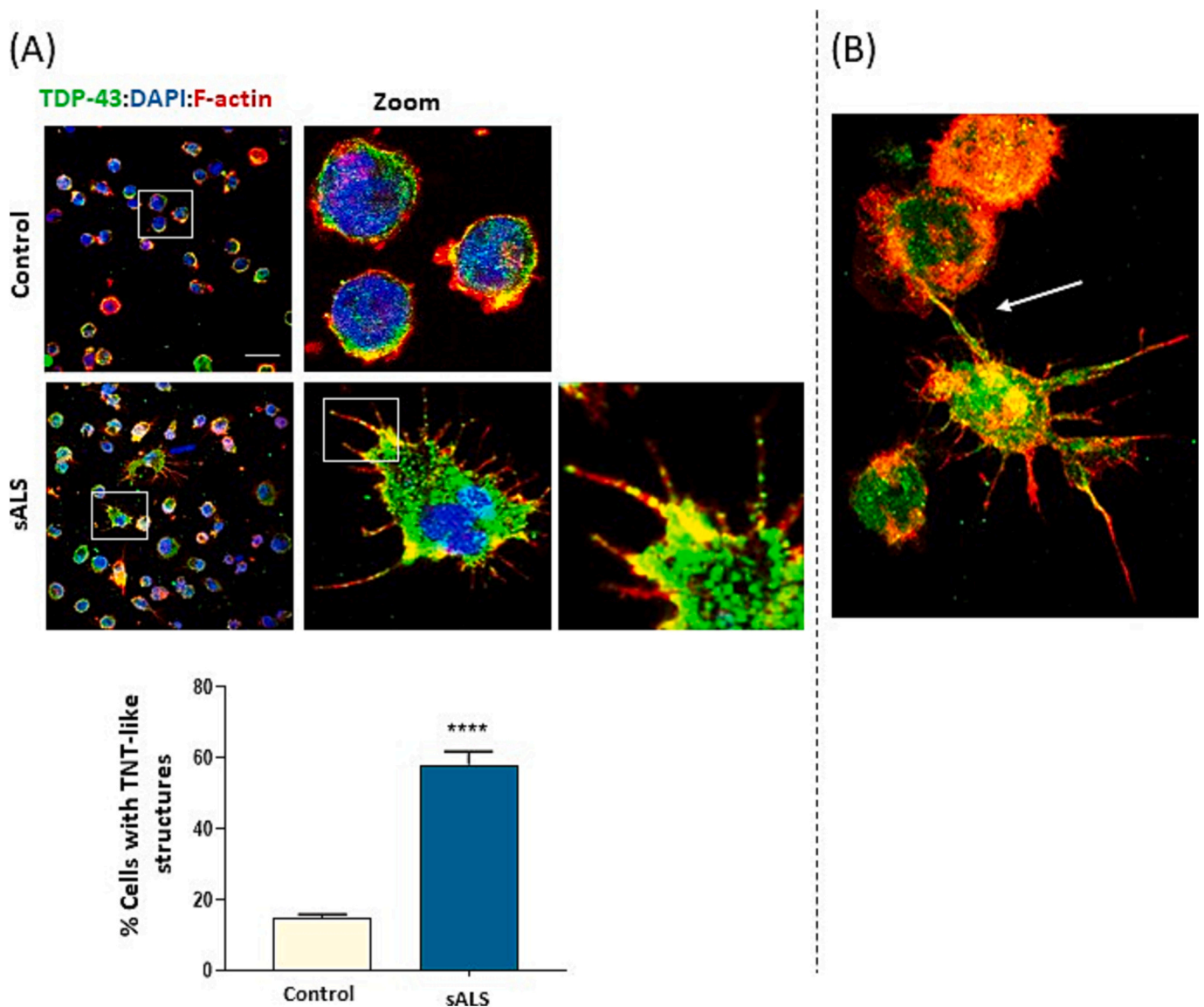


Fig. 1. Cell structure analysis in lymphoblasts from control and sALS patients. Cells were stained with TDP-43 antibody (green), phalloidin (red) and DAPI (blue). A) Representative immunofluorescence images depict cytoskeleton protrusion, which are frequently observed in sALS cells. The graph illustrates the percentage of cells with F-actin protrusions (TNT-like structures) measured in 8 sALS and 5 controls samples, with at least 4 fields of view for each subject. B) Representative image demonstrate cell-to-cell communication *via* TNT-like structures, where TDP-43 is localized. Scale bars, 20 μm . Data are presented as mean \pm SEM. Statistical analysis was conducted using the Student's *t*-test(*****p* < 0.0001). (For interpretation of the references to colour in this figure legend, the reader is referred to the web version of this article.)

like structures in ALS lymphoblasts (Fig. 1A) for the first time. The percentage of ALS cells displaying these structures is significantly higher than in control cells (Fig. 1A). Furthermore, in the merged images, we observed TDP-43 co-localization with the TNTs. In the extracellular medium surrounding these TNT-like structures, a notable abundance of green puncta consistent with TDP-43 staining was also observed. Moreover, despite the lymphocyte cells' non-adherent nature, we detected sporadic cell-to-cell connections through the tunneling nanotubes when cells were fixed for immuno-cytochemistry analysis (Fig. 1B).

3.2. TDP-43 is secreted into the extracellular medium and may contribute to the spread of pathology to healthy cells

The extracellular medium from control and sALS lymphoblasts cells was collected after 72–96 h of culture and tested for the presence of full-length or fragmented TDP-43 by WB analysis. Primarily, we observed a 25 KDa fragment localized in the extracellular media from 80% of ALS patients' lymphoblasts analyzed (Fig. 2A). Subsequently, conditioned medium (CM) from control and sALS patient-derived lymphoblasts was added to control healthy cells for 72 h to investigate the potential dissemination of TDP-43 pathology. Using immunochemistry and confocal microscopy, we observed TDP-43 mislocalization in control cells treated with CM from sALS lymphoblasts, leading to an increase in its cytosolic presence (Fig. 2B). Furthermore, F-actin staining with

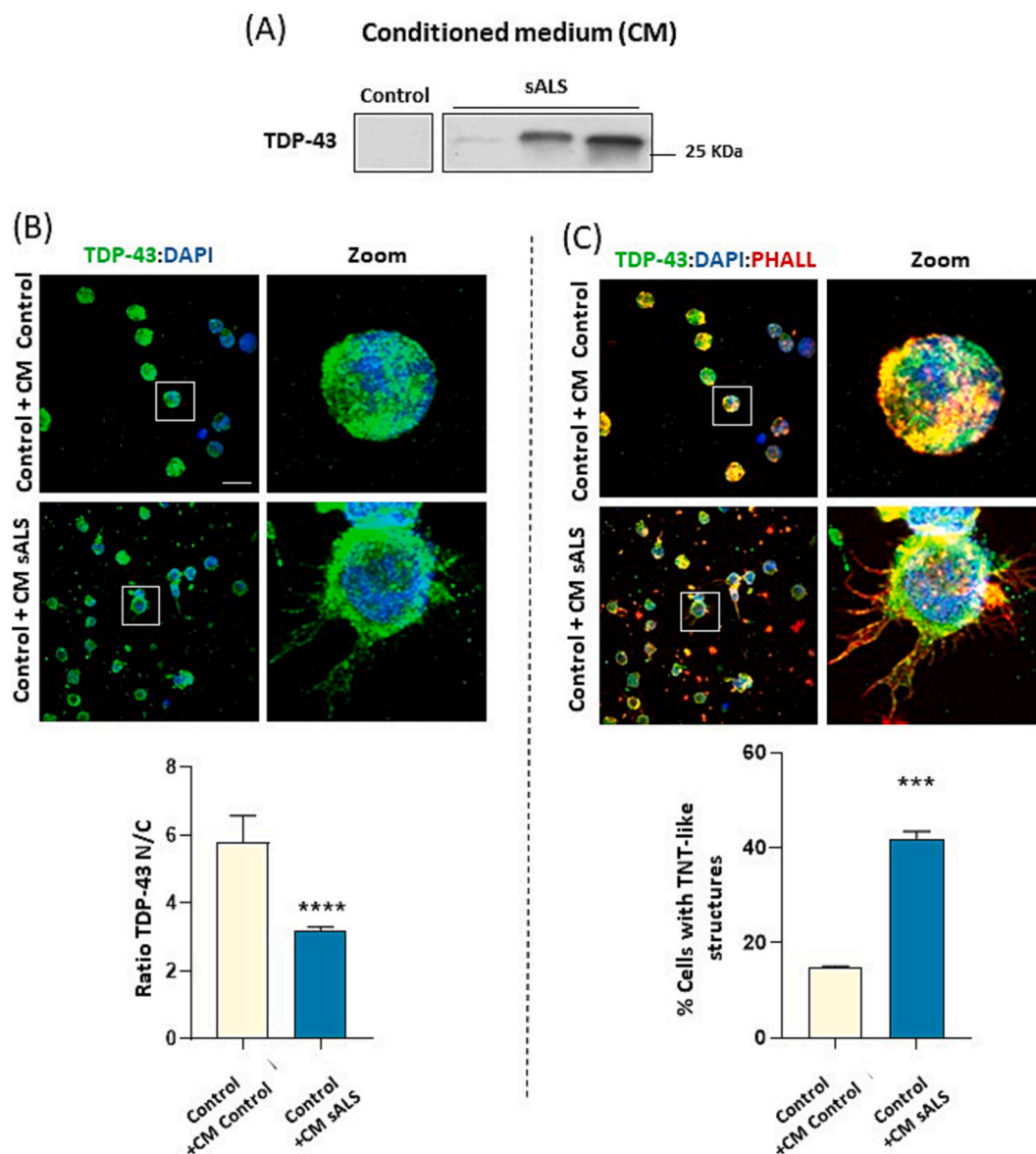


Fig. 2. Conditioned medium (CM) from sALS lymphoblasts induces TDP-43 pathology in control cells. A) A representative immunoblot depicts a 25 KDa fragment of TDP-43 in the extracellular medium of sALS cells. B, C) Representative immunofluorescence images of control lymphoblasts exposed to CM from sALS or control cells for 72 h stained with TDP-43 antibody (green), phalloidin (red) and DAPI (blue), B) TDP-43 localization is represented as TDP-43 nucleo-cytoplasm ratio (mean nuclear intensity divided by the mean cytoplasmic intensity) using Image J software for quantification, C) TNT-like structures induced in control cells with CM of sALS cells. The percentage of cells with F-actin protrusions (TNT-like structures) and TDP-43 localization were measured in at least 4 fields of view. Scale bars, 20 μ m. Data are expressed as mean \pm SEM of three independent experiments performed on 3 different controls exposed to CM from 4 sALS and 3 control lymphoblastoid lines. Statistical analysis was performed using the Student's *t*-test (***p* < 0.001, ****p* < 0.0001). (For interpretation of the references to colour in this figure legend, the reader is referred to the web version of this article.)

phalloidin revealed cytoskeleton changes with the formation of TNT-like structures (Fig. 2C), whereas CM from control lymphoblasts has no significant effects. Finally, WB and immunofluorescence analyses detected an increase in phosphorylated TDP-43 levels, both in full-length and in their 35 and 25 KDa fragments (Fig. 3A and B), in control cells treated with CM from sALS lymphoblasts. These results collectively suggest propagation of TDP-43 pathology.

Next, we investigated whether CM from sALS cells could also be pathogenic for other cell types. CM from two different controls and from two sALS was incubated for 72 h with healthy myoblasts, obtained from a muscle biopsy of a healthy individual during surgery for bone fractures

in two independent experiments. Immunohistochemistry showed an increase in cytoplasmic TDP-43 and phosphorylated TDP-43, together with actin cytoskeleton changes, compared to myoblasts treated with CM from healthy lymphoblasts (Fig. 4).

Osteosarcoma USO2 cells were selected next because of their larger cytoplasm, which allows for better investigation of various cytoplasmic events and functions. Here, we demonstrate how treatment of USO2 cells with CM from sporadic ALS patients for 72 h is also able to induce TDP-43 pathology in this cell line, leading to TDP-43 mislocalization and formation of aggregates (Fig. 5A). Moreover, we explored whether TDP-43 pathology may alter the interaction between tubulin and the

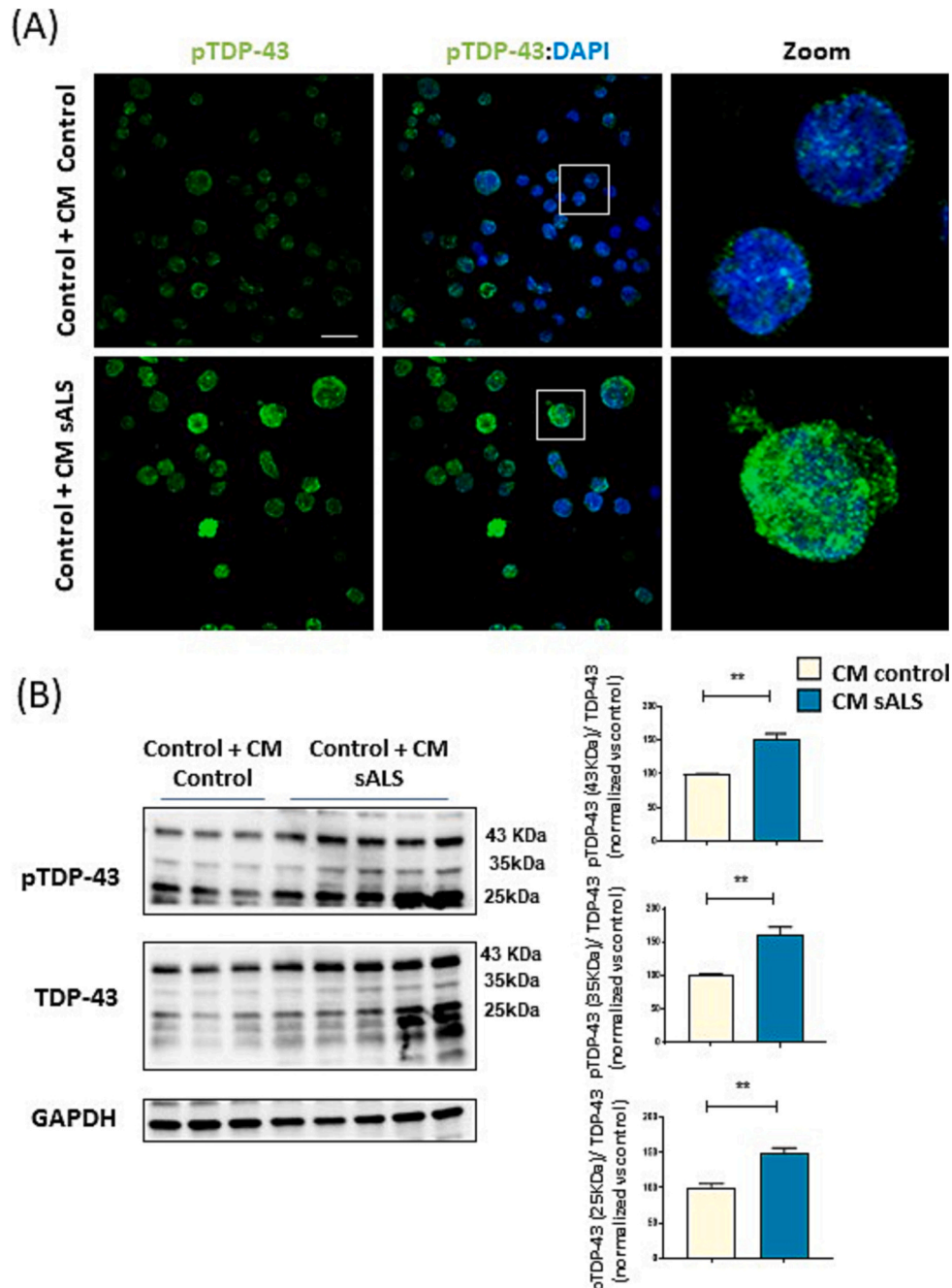


Fig. 3. TDP-43 phosphorylation status in control lymphoblasts after exposure to CM from sALS or control individuals for 72 h. A) Representative immunofluorescence images of cells stained with a pTDP-43 antibody (green) and DAPI (blue). Scale bars, 20 μm. B) Representative immunoblot and quantification of phosphorylated TDP-43 (full-length, or 35 and 25 KDa fragments). Data are expressed as mean ± SEM of three independent experiments performed on 2 healthy cell lines with CM from 5 sALS and 3 controls. Statistical analysis was conducted using the Student's t-test (**p < 0.01). (For interpretation of the references to colour in this figure legend, the reader is referred to the web version of this article.)

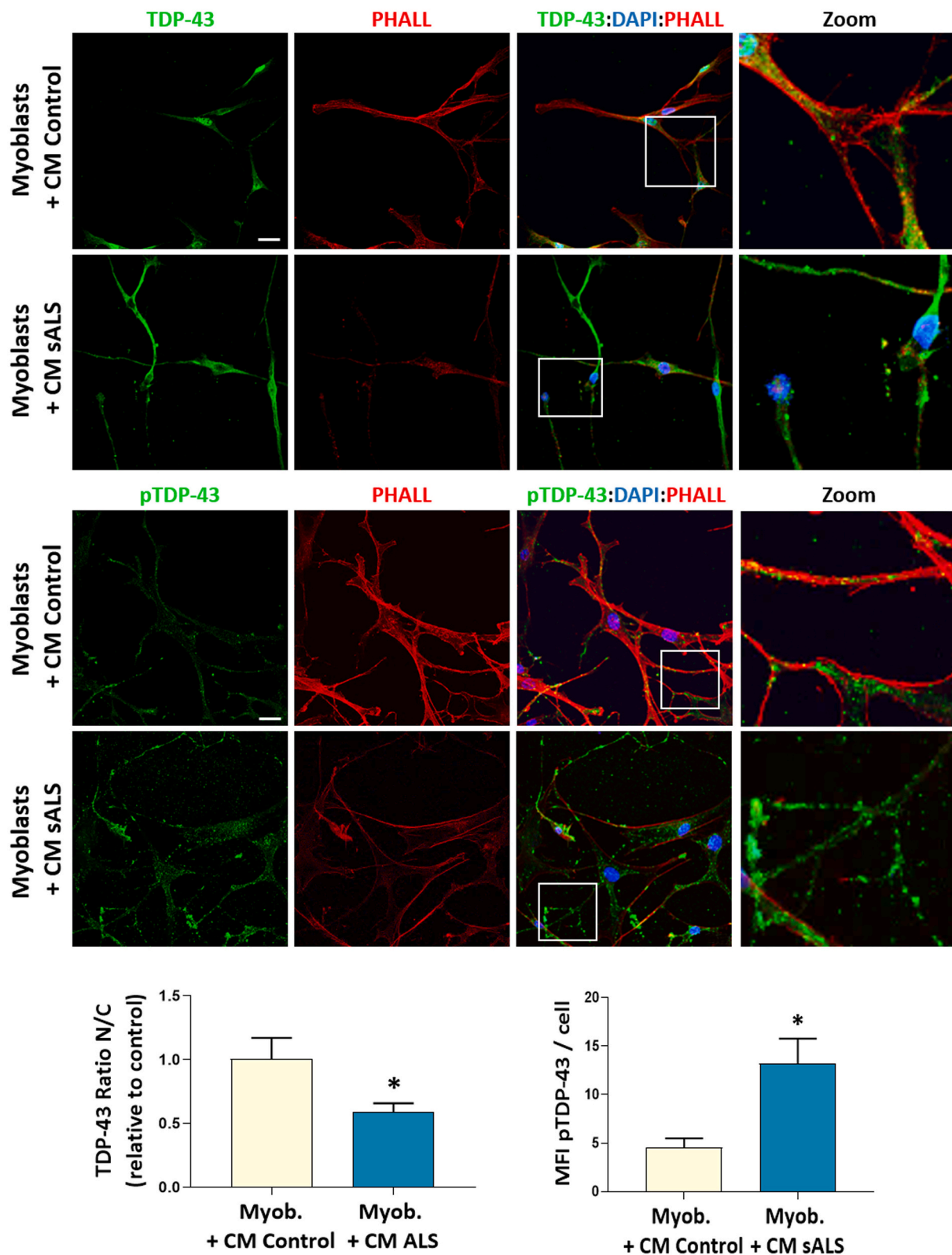


Fig. 4. Pathogenic behavior of CM from sALS cells in human myoblasts. Depletion of TDP-43 from nucleus to the cytoplasm is observed along with an increase in phosphorylation. Representative immunofluorescence images of cells stained with TDP-43 or p-TDP43 antibodies (green), phalloidin (red) and DAPI (blue). TDP-43 localization is quantified as TDP-43 nucleo-cytoplasm ratio, and TDP-43 phosphorylation status is measured as the pTDP-43 mean fluorescence intensity (MFI). Scale bars, 25 μ m. Image analysis was performed in at least 4 fields of view using Image J software. Data are expressed as mean \pm SEM of two independent experiments performed with CM of 2 sALS and 2 controls on naïve recipient myoblasts. Statistical analysis was performed using the Student's *t*-test (**p* < 0.05). (For interpretation of the references to colour in this figure legend, the reader is referred to the web version of this article.)

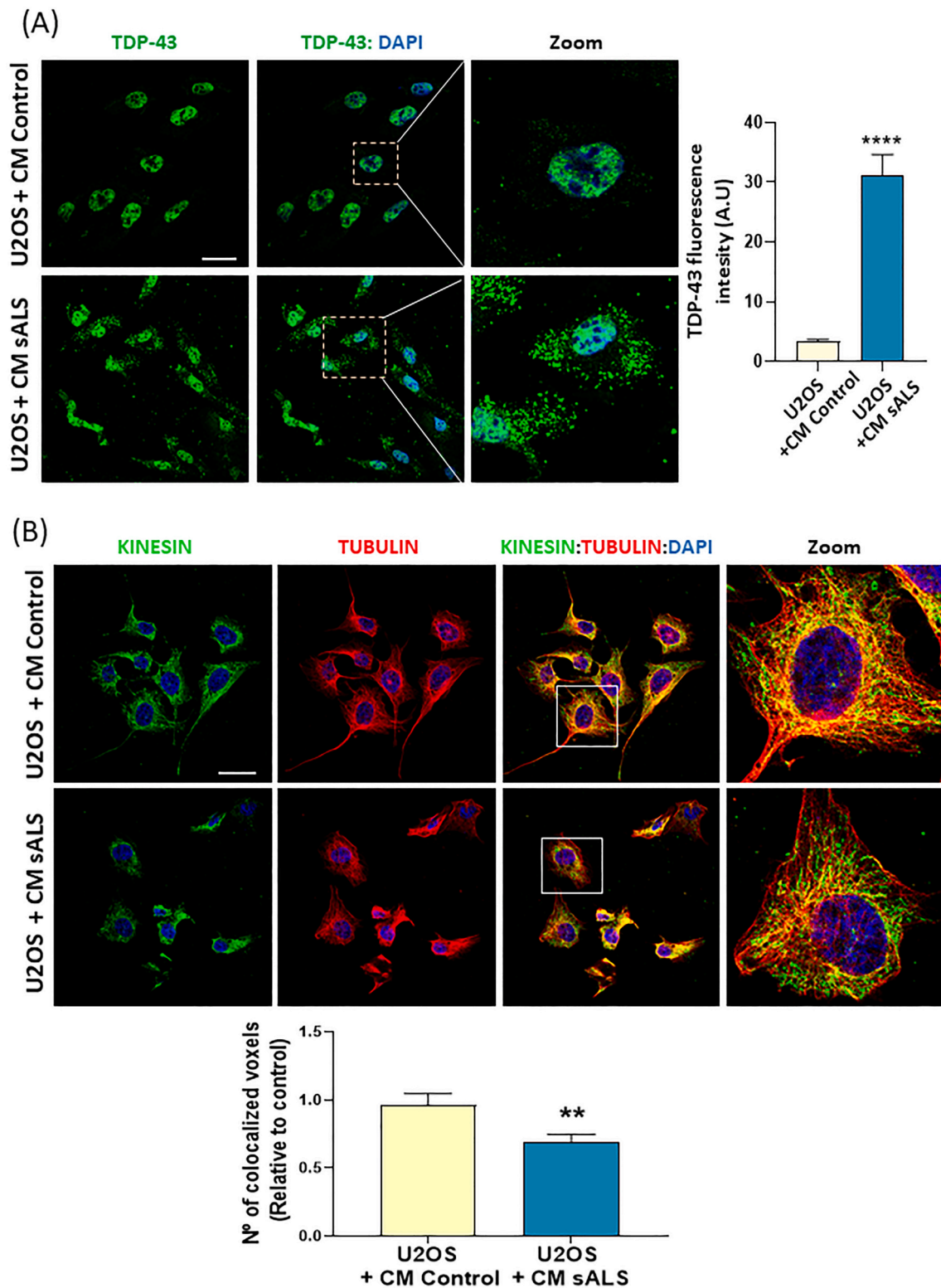


Fig. 5. Conditioned medium from sALS lymphoblasts induces TDP-43 pathology in U2OS osteosarcoma cells. A) Representative immunofluorescence images of TDP-43 (green) and DAPI staining (blue) in U2OS cells treated with CM of control or sALS lymphoblasts for 72 h. (A.U, arbitrary units). Scale bar, 40 μ m. Data are expressed as mean \pm SEM of three independent experiments performed with CM from 4 sALS and 3 controls on naïve recipient U2OS cells. B) Confocal immunofluorescence images of cells stained with kinesin (green) and tubulin (red) antibodies and DAPI (blue). Scale bar, 40 μ m. TDP-43 fluorescence analysis was performed in at least 4 fields of view for each condition using Image J software and kinesin-tubulin colocalization data are from four experiments performed with CM from 2 sALS and 2 controls in at least 3 fields of view for each condition, using Image J software. Statistical analysis was performed using the Student's t-test (** $p < 0.01$, **** $p < 0.0001$). (For interpretation of the references to colour in this figure legend, the reader is referred to the web version of this article.)

transport motor kinesin (Liu and Henty-Ridilla, 2022). Immunocytochemistry staining of both kinesin and tubulin showed a significant decrease in the co-localization of these two proteins (Fig. 5B) in U2OS cells after induction of TDP-43 pathology by treatment with the CM from sALS patients.

3.3. Extracellular vesicles isolated from conditioned medium of sporadic ALS lymphoblasts may propagate TDP-43 pathology

EVs were isolated using total exosome isolation reagent from the CM of controls and sALS lymphoblasts cultured in medium with exosome-depleted FBS. We then analyzed the relative abundance of TDP-43 species (full size and fragmented) in EVs from controls and sALS samples by WB, using antibodies against the N- or C-terminus of TDP-43. A fragment of 25 kDa was identified in the EVs fraction from sALS by using an anti C-terminal TDP-43 antibody (Fig. 6A).

Subsequently, 30 μ L of the isolated EVs in PBS were used to treat control lymphoblasts for 72 h. The EVs fraction from sALS, but not the one from control lymphocytes, was able to induce the TDP-43 pathology (cytoplasmic localization, TNT-like structures, increase in TDP-43 phosphorylation) (Fig. 6B and C).

3.4. The CK-1 inhibitor IGS2.7 prevents the propagation of TDP-43 pathology

Treatment with the benzothiazole-based CK-1 inhibitor IGS2.7 has demonstrated the restoration of TDP-43 pathology in both cell cultures and animal models (Alquezar et al., 2016) (Martínez-González et al., 2020). Thus, we selected this CK-1 inhibitor to investigate its potential to inhibit, stop or decrease TDP-43 propagation. sALS lymphoblasts were treated for 72 h with IGS2.7 at a fixed dose of 5 μ M, and the cell culture media were collected (ptCM). When control lymphoblasts were incubated in the presence of CM from IGS2.7 treated sALS cells, TDP-43 pathology was not observed (Fig. 7). In fact, TDP-43 remained localized in the nucleus (Fig. 7A-B), p-TDP-43 did not increase in full-length or fragmented forms (Fig. 7D-E), and the cytoskeleton did not form TNT-like nanotubes (Fig. 7A-C).

Next, we investigated whether TDP-43 pathology could also be propagated to neuronal cells and inhibited by IGS2.7. We confirmed that CM from sALS lymphoblasts is also capable of propagating TDP-43 pathology in the neuronal cell line SH-SY5Y (Fig. 8). In this case, similar TDP-43 pathology is observed (*i.e.* an increase of TDP-43 aggregates in the cytoplasm and hyperphosphorylation). Additionally, propagation is also prevented when these neuronal cells are incubated with CM of sALS lymphoblasts previously treated with the CK-1 inhibitor IGS2.7.

To characterize the secretome of sALS lymphoblastoid cell lines capable of propagating TDP-43 pathology, we isolated an enriched fraction of EVs by precipitation and determined the concentration and size of the vesicles in control and sALS cells with and without treatment (Fig. 9). Our results demonstrate a statistically significant increase in the concentration of EVs in the precipitated fraction from CM of sALS patients, which is reduced upon treatment with IGS2.7 (Fig. 9A-B). In addition, we observed a not significant trend towards an increase in the size (mode) of the analyzed fraction, which was reduced upon IGS2.7 treatments (Fig. 9C). Taken together, these results suggest that IGS2.7 may halt the propagation of cellular TDP-43 pathology.

Finally, to correlate TDP-43 pathology with functional alterations in recipient cells, we utilized the larger cytoplasm of U2OS cells compared to lymphoblasts to analyze whether induced TDP-43 pathology was associated with deficient intracellular transport in ALS. For this purpose, we monitored the anterograde transport mediated by kinesin using a chemical probe containing the cyanine fluorophore Cy5, Cy5-KBP, previously employed in our laboratory (Oliva et al., 2022). In these experiments, U2OS cells were treated with CM from healthy lymphoblasts and from sALS patients for 72 h. Cy5-KBP movies were analyzed with ImageJ, and resultant trajectories were further analyzed and

represented by colour according to their mean track displacement (shorter in blue, larger in red) (Fig. 10A, B, C). A significant reduction in the average displacement of Cy5-KBP particles was observed in U2OS cells treated with CM from sALS cells compared to those treated with CM from healthy controls (Fig. 10D). However, this treatment did not alter the other two parameters analyzed, mean and maximal track velocity (Fig. 10E, F). These results indicate the ability of CM from sALS cells, which promote TDP-43 pathology, to induce a functional deficit in intracellular transport in healthy cells. When U2OS cells were treated with CM from ALS lymphoblasts previously treated with IGS2.7, no significant alteration in the mean track displacement of Cy5-KBP movement was observed (Fig. 10G), demonstrating the potential of this drug not only to rescue TDP-43 mislocalization but also to improve cellular functionality such as intracellular transport.

4. Discussion

Neurodegenerative diseases are frequently referred to as proteinopathies (Bayer, 2015). Various proteins such as alpha-synuclein, beta-amyloid, tau or TDP-43 undergo different post-translational modifications, with misfolded conformations being the main hallmarks of Parkinson's and Alzheimer's diseases, ALS and frontotemporal dementia, respectively (Wilson 3rd et al., 2023). Furthermore, several studies indicate a prion-like spreading of these protein aggregates as the mechanism involved in the progression of these diseases (Polymenidou and Cleveland, 2012). Although robust information has been gathered regarding several of the abovementioned proteins (Vargas et al., 2019; Ayers et al., 2018), the mechanism of TDP-43 propagation remains relatively unknown.

TDP-43 aggregates are present in >97% of ALS patients, and the restoration of functional homeostasis of TDP-43 has been proposed as an effective therapeutic approach for ALS (Hayes and Kalab, 2022). In our team, we have developed a patient-based cellular model where TDP-43 pathology is well recapitulated (Posa et al., 2019). Immortalized lymphocytes from ALS patients offer an excellent platform to study the molecular mechanisms of TDP-43 and to discover new drugs capable of modulating this key protein. In fact, we have previously reported how these ALS lymphoblasts show an increase in TDP-43 migration to the cytoplasm, along with higher protein phosphorylation, both in the full length and in their 35 and 25 kDa fragments (Posa et al., 2019).

Here, we report cytoskeletal changes in immortalized ALS lymphocytes. Tunneling nanotubes (TNTs) or TNT-like structures are significantly increased in sALS cells compared to healthy controls cells. Similar cytoskeleton alterations have been previously found in TDP-43 positive cells from severe Alzheimer's disease patients. (Cuevas et al., 2022) The molecular mechanisms involved in TNT formation are not yet well known, but it is believed that cellular stress could be a key player. (Wang et al., 2011) In general, these F-actin structures play a crucial role in cell communication, acting as *intercellular bridges that mediate the transfer of various cellular cargos* (Cordero Cervantes and Zurzolo, 2021). *They are involved in tau and alpha-synuclein spreading* (Lagalwar, 2022; Chakraborty et al., 2023), *and in the case of sALS lymphoblasts they may be involved in the transport of TDP-43 to other cells. TDP-43 co-localizes with the TNT-like structures and could potentially serve as a release route to the extracellular medium or penetrate other cells through direct cell-to-cell communication via these TNT-like protrusions.*

TDP-43 pathology propagation was further supported by our observation that conditioned medium obtained from lymphoblasts derived from sALS patients is able to enhance TDP-43 phosphorylation and mislocalization of TDP-43 in control lymphoblasts. Furthermore, changes in the cytoskeleton are also induced, leading to the formation of TNT-like structures. These results are consistent with previous findings where the extracellular medium from cells overexpressing TDP-43 perturbed healthy cells resulting in cytotoxicity and metabolic changes (Hergesheimer et al., 2020). Moreover, in the study reported here, the prion-like behavior of TDP-43 was further confirmed in other cell types

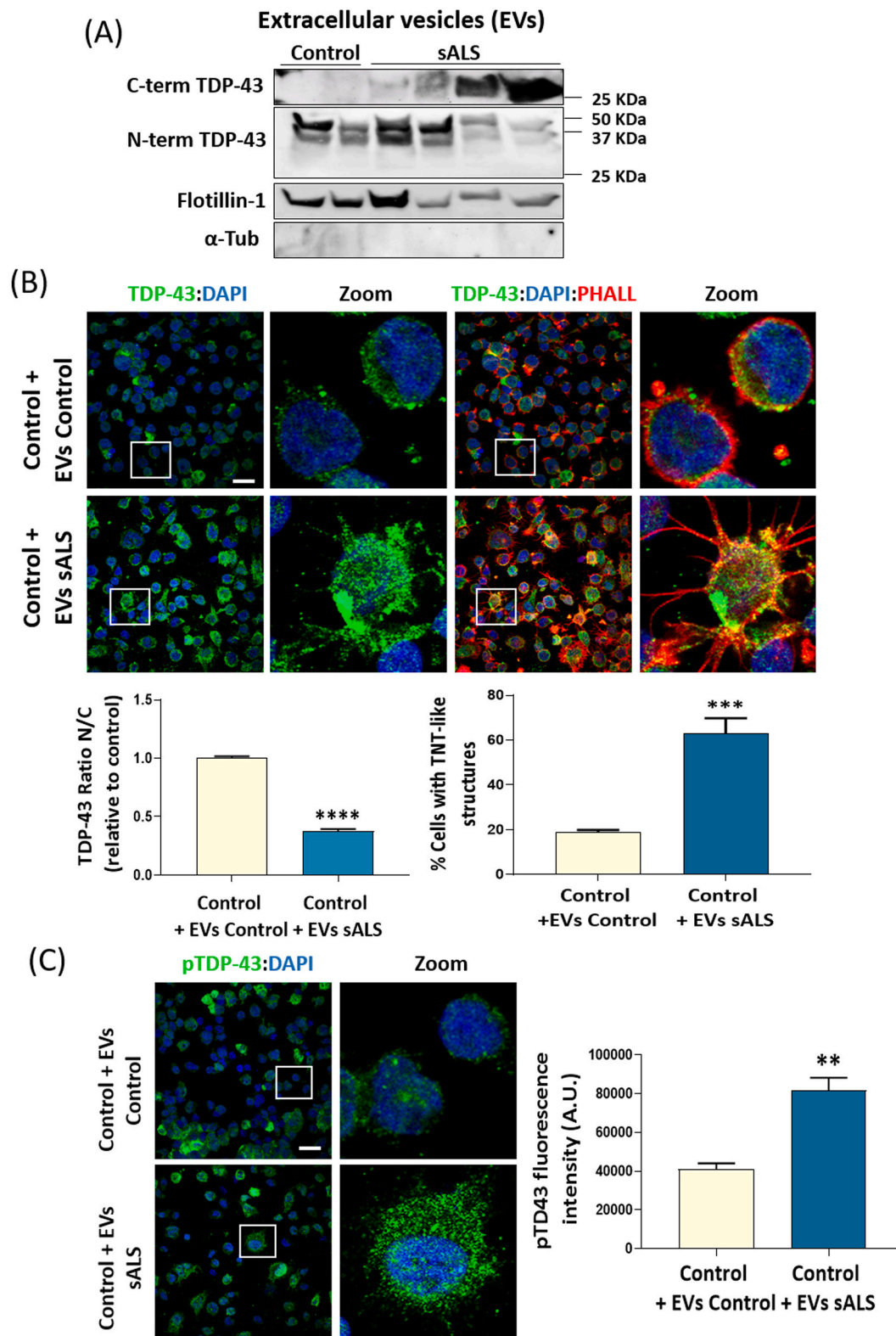


Fig. 6. Extracellular vesicles (EVs) from sALS lymphoblasts induce TDP-43 pathology in control cells. (A) Western blot analysis of C-terminal fragment or full-length TDP-43 in isolated EVs from the indicated samples. α -tubulin was used as negative control for EVs, and Flotillin-1 as positive control. B, C) Representative immunofluorescence images of control lymphoblasts cultured in presence or absence of EVs of sALS cells for 72 h stained with TDP-43 and pTDP-43 antibodies (green), phalloidin (red) and DAPI (blue). Scale bars, 20 μ m. B) TDP-43 localization (represented as the TDP-43 nucleo-cytoplasmic ratio), the percentage of cells with F-actin protrusions (TNT-like structures), and C) pTDP-43 immunofluorescence intensity (A.U., arbitrary units) were measured in at least 4 fields of view using Image J software. Data are expressed as mean \pm SEM of two independent experiments performed on 2 different control lymphoblasts exposed to EVs from 1 sALS and 1 control lymphoblastoid lines. Statistical analysis was performed using the Student's t-test (** $p < 0.01$, *** $p < 0.001$, **** $p < 0.0001$). (For interpretation of the references to colour in this figure legend, the reader is referred to the web version of this article.)

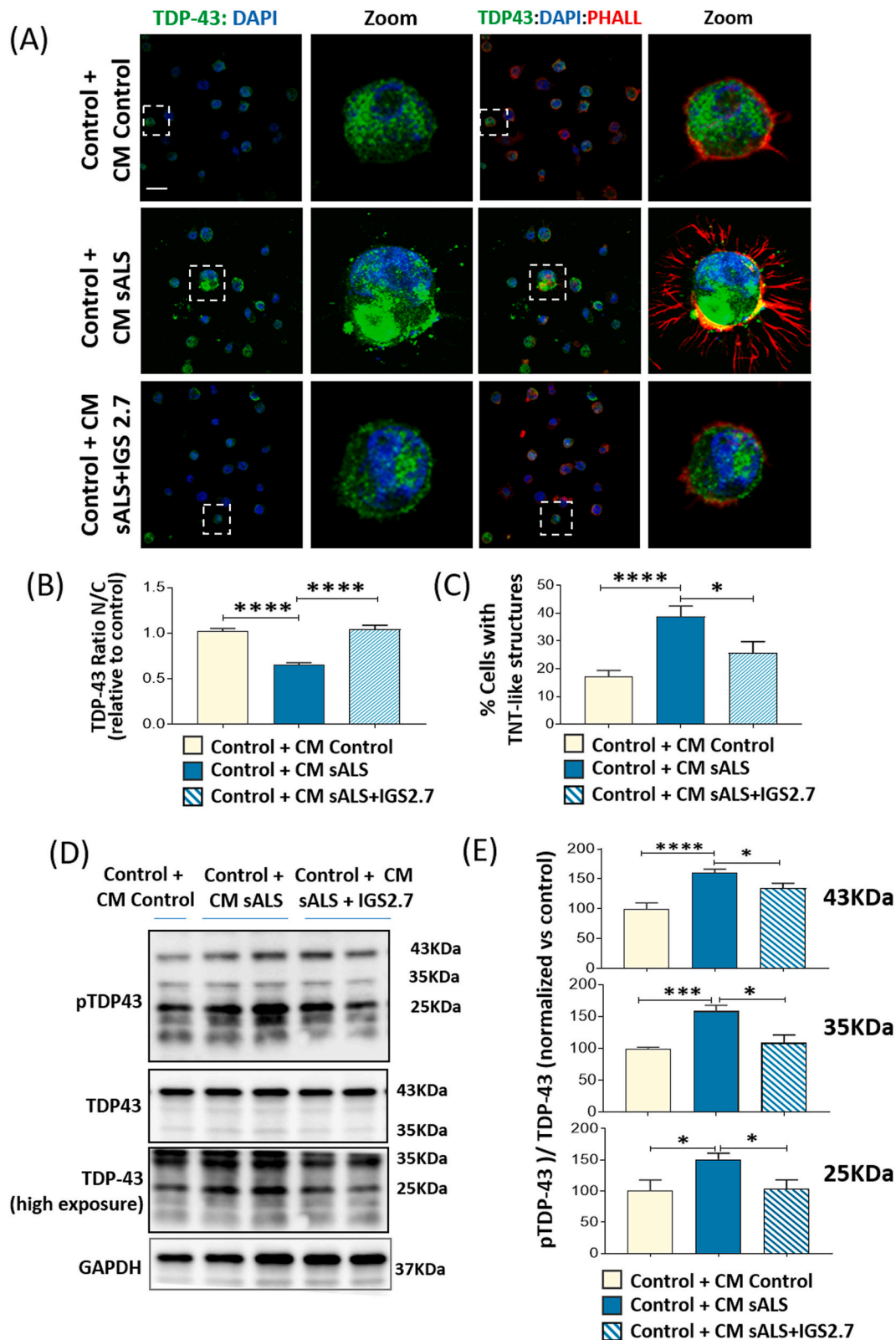


Fig. 7. Healthy lymphoblasts treated with CM from healthy donors and sALS patients pre-treated or not with IGS2.7 (5 μ M) for 72 h. A) Representative immunofluorescence images of cells stained with TDP-43 antibody (green), phalloidin (red) and DAPI (blue). B) TDP-43 localization analysis represented as TDP-43 nucleocytoplasmic ratio. C) TNT-like structures analysis. The graph represents the percentage of cells with F-actin protrusions (TNT-like structures). Measurements were performed cell-to-cell in at least 4 fields of view using Image J software. Scale bars, 20 μ m. D, E) Representative immunoblot and quantification of full-length, 35 and 25 KDa p-TDP-43 fragments using a phospho-specific anti-TDP-43 antibody. Bars are the mean \pm SD of independent experiments performed in 2 healthy cell lines with CM or pt-CM from 3 sALS or CM from 2 control lymphoblastoid cells. Statistical analysis was performed using One-way ANOVA followed by Bonferroni's post-test (* p < 0.05, *** p < 0.001, **** p < 0.0001). (For interpretation of the references to colour in this figure legend, the reader is referred to the web version of this article.)

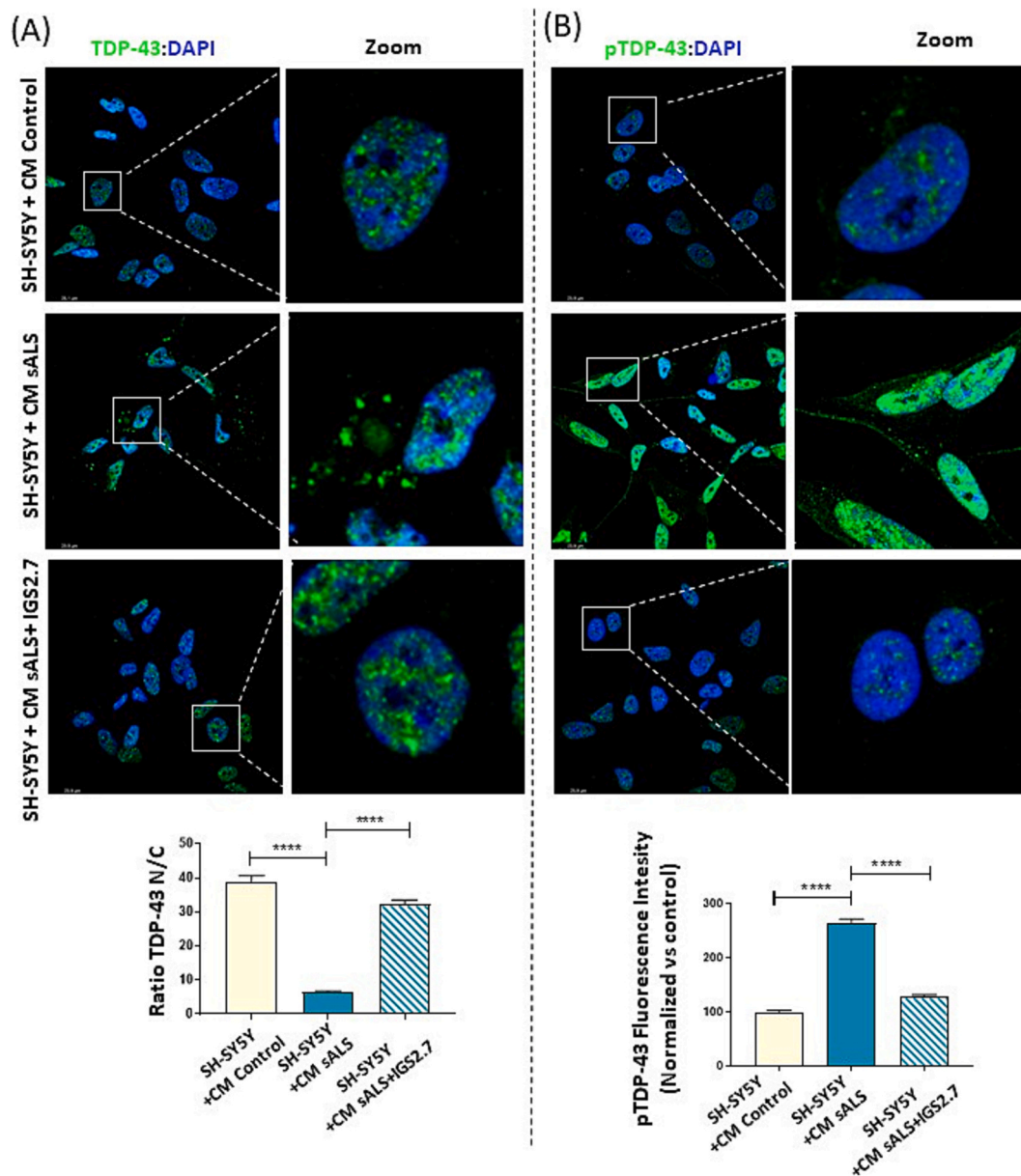


Fig. 8. Neuroblastoma cell line SH-SY5Y treated with CM from 2 healthy donors and 2 sALS patients pre-treated or not with IGS2.7 (5 μ M) for 72 h. Representative immunofluorescence images of cells stained with either TDP-43 or p-TDP43 antibodies (green) and DAPI (blue). A) TDP-43 localization is represented as the TDP-43 nucleocytoplasmic ratio. B) pTDP-43 fluorescence intensity is represented normalized versus control. Measurements were performed cell-to-cell in at least 4 fields of view using Image J software. Statistical analysis was performed using One-way ANOVA followed by Bonferroni's post-test. (**** $p < 0.0001$). (For interpretation of the references to colour in this figure legend, the reader is referred to the web version of this article.)

such as human myoblasts, the neuroblastoma cell line SH-SY5Y and the U2OS osteosarcoma human cell line, as conditioned medium from sALS lymphoblasts induced characteristic pathological TDP-43 features. Interestingly, this pathological phenotype is not induced when CM from control lymphoblasts is used. These results are consistent with the reported effect of CSF derived from ALS-FTD patients inducing TDP-43 pathology in U251 glioblastoma cells *via* TNT and exosomes (Ding et al., 2015), or the effect of ALS spinal cord extracts spreading TDP-43 pathological features in cerebral organoids (Tamaki et al., 2023). Together, these results suggest that ALS-derived TDP-43 is capable of spreading pathology among cells.

In several neurodegenerative diseases, the release of misfolded proteins from affected cells into the extracellular medium has been reported. The discharge may occur either as free proteins or incorporated into lipid bilayer-delimited vesicles (EVs), which can be taken up by

other cells, contributing to the spread of the disease (Casarotto et al., 2022). *In this study*, we collected extracellular medium from both control and ALS lymphoblasts, as well as an enriched EVs fraction, to evaluate whether the secretion of TDP-43 protein (full size and fragmented) differed in ALS cells. We indeed observed a higher expression of the 25 kDa TDP-43 fragment in the EVs derived from sALS patients. Moreover, nanoparticle tracking analysis (NTA) revealed that the concentration of EVs from ALS cells was statistically higher than that of EVs derived from control cells. Taken together, these results suggest that EVs may also play a key role in the propagation of TDP-43 pathology.

We have previously reported the efficacy of various protein kinase inhibitors, including GSK-3, CK-1, CDC7, and TTBK1 inhibitors, in mitigating TDP-43 pathology in both cell cultures and *in vivo* models (Vaca et al., 2021; Martínez-González et al., 2021; Nozal et al., 2022; Salado et al., 2014). Particularly, the CK-1 inhibitor known as IGS2.7 has

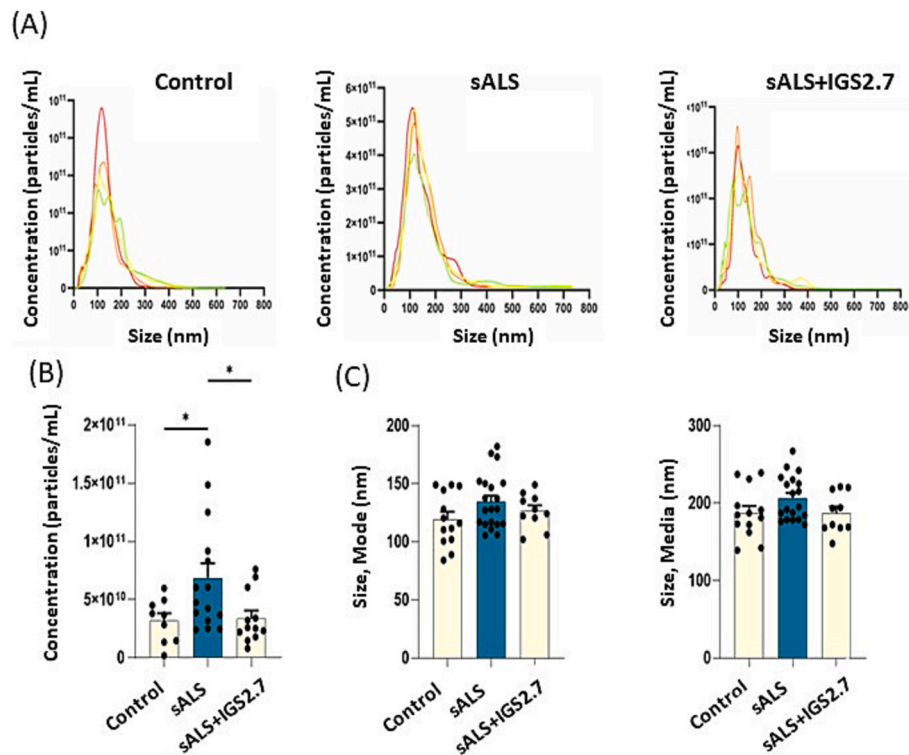


Fig. 9. Extracellular vesicles characterization of the sALS and control lymphoblastoid cell lines in the presence or absence of IGS2.7 (5 μ M). A) Representative concentration and sizes of particles measured from the precipitated fraction of control, sALS and treated sALS lymphoblastoid media. B) Particle concentration and C) size. Data are expressed as mean \pm SEM of three independent experiments performed with 3 different control lymphoblasts and 5 sALS lymphoblastoid lines with and without IGS2.7 treatments. Statistical analysis by one-way ANOVA followed by Dunnett's *post hoc* test (* $p < 0.05$).

demonstrated the ability to reduce TDP-43 phosphorylation and restore nuclear localization in lymphoblasts derived from ALS and frontotemporal dementia patients (Alquezar et al., 2016). Moreover, chronic treatment of IGS2.7 in TDP-43 transgenic mice resulted in motor neuron preservation and decreased levels of microglial reactivity, astrogliosis and p-TDP-43 levels in the spinal cord of the animals (Martínez-González et al., 2020). Our current data indicate that treatment of sALS lymphoblasts with the CK-1 inhibitor named IGS2.7, a small benzothiazole derivative, effectively prevents the dissemination of TDP-43 pathology. Specifically, when control lymphoblasts were exposed to CM from sALS cells treated with IGS2.7 (ptCM), TDP-43 phosphorylation remained unchanged, and the protein localization remained primarily nuclear. Additionally, we observed no cytoskeleton changes or alteration in the size and abundance of EVs isolated from pre-treated ALS cells. Furthermore, this effect was also observed when neuronal cells SH-SY5Y were cultured with CM from IGS2.7-treated sALS cells.

Finally, it is well-established that microtubule-based intracellular transport mediated by kinesin motors is crucial for the structural and functional organization of cells. Protein aggregates disrupt microtubule dynamics, affecting the balance of molecular motors like kinesin, and contributing to a spectrum of diseases (Soo et al., 2011). Moreover, dysfunctions in cellular trafficking, including abnormalities in the molecular motors dynein and kinesin, have been widely implicated in ALS (Burk and Pasterkamp, 2019). Hence, we sought to investigate whether altered phosphorylation and truncation of TDP-43 protein could contribute to the impaired kinesin-mediated intracellular transport in ALS. To this end, we monitored intracellular transport in human osteosarcoma U2OS cells after inducing TDP-43 pathology by treating them with conditioned medium from sporadic ALS cells, as described previously. Our findings support the notion that TDP-43 pathology indeed disrupts intracellular transport. Interestingly, when U2OS cells were exposed to ptCM from sALS cells treated with IGS2.7, cellular transport was restored to normal rates, and the number of TDP-43 aggregates was

also diminished.

5. Conclusion

Altogether, our data demonstrate the significant therapeutic potential of CK-1 inhibitors, particularly the small heterocyclic molecule known as IGS2.7. These inhibitors not only in restore the functional homeostasis of TDP-43 pathology in patients but also prevent disease transmission among different cell types. Translating the use of this small molecule to clinical practice would enable us to investigate whether these results hold true in humans and whether TDP-43 dissemination among healthy cells could be effectively reduced.

Funding

Funding support from La Caixa and Luzón Foundation (grant no. HR21-00931), MCIN/AEI /10.13039/501100011033 (grant no. PID2019-105600RB-I00 to A.M. and E.P.C. and PID2021-128340OA-I00, CNS2022-135852 and RYC2019-027489-I to V.P.), Consejo Superior de Investigaciones Científicas (PTI+ Neuroaging, European Union Next Generation EU/PRTR), Spanish Health Institute Carlos III (grant no. CB18/05/00040 to E.P.C, L.M-G, C. T-B., V.P., A.M.R. and A.M.) and Ministerio de Educación (grant no FPU18/06310 to C.T.B.) are acknowledged.

CRedit authorship contribution statement

Eva P. Cuevas: Writing – review & editing, Visualization, Methodology, Investigation, Formal analysis. **Loreto Martínez-González:** Writing – review & editing, Validation, Methodology, Investigation, Formal analysis. **Clara Gordillo:** Investigation, Formal analysis. **Carlota Tosat-Bitrián:** Writing – review & editing, Methodology, Investigation. **Carmen Pérez de la Lastra:** Writing – review & editing, Methodology,

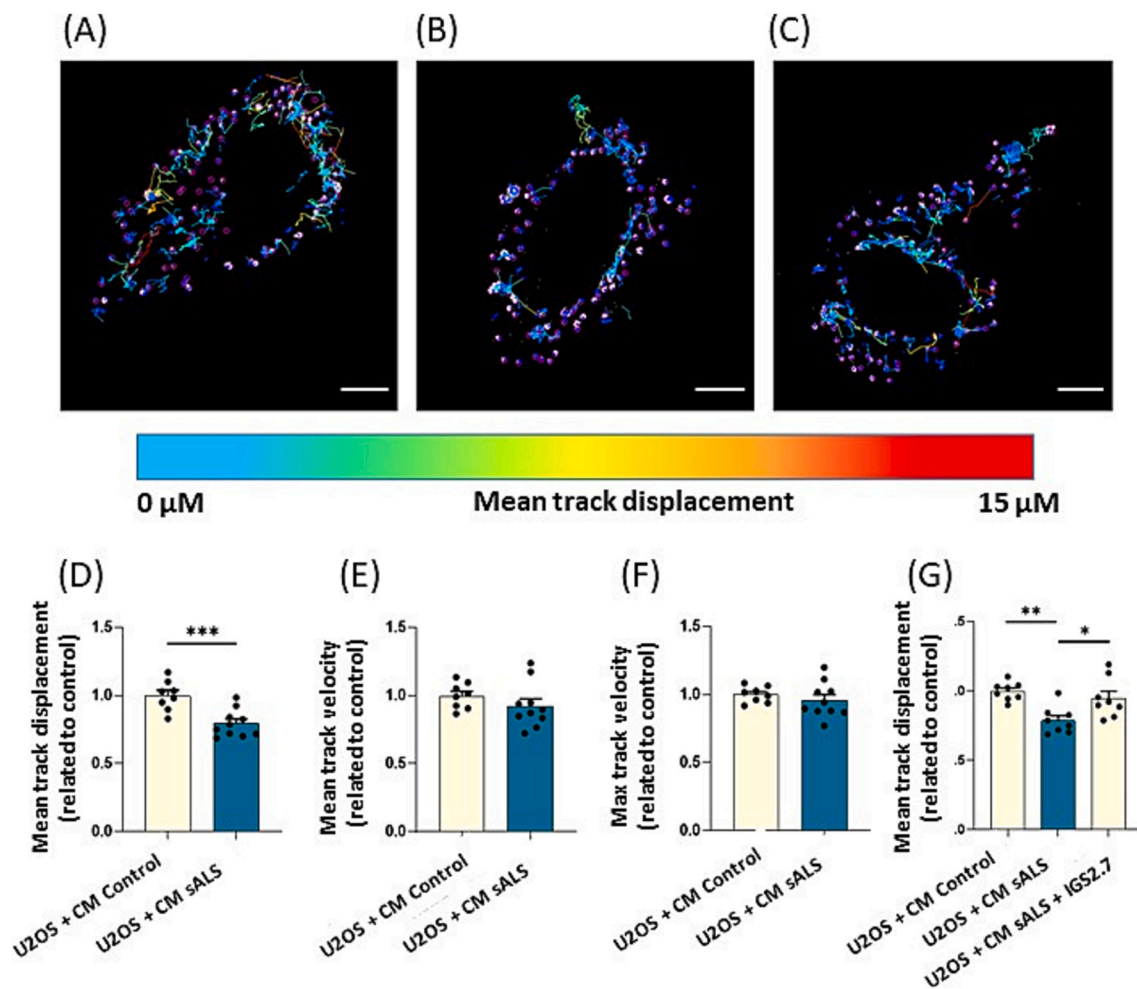


Fig. 10. Intracellular transport alterations induced by TDP-43 pathology in U2OS cells. Cy5-KBP trajectories in naive recipient U2OS cells treated with CM of lymphoblasts from A) 1 healthy subject, B) 2 sALS patients and C) 2 sALS patients treated with the IGS2.7 were analyzed and colored by the mean track displacement. Scale bars, 10 μ m. Trajectories were analyzed according to three different parameters, D, G) mean track displacement, E) mean track velocity and F) maximal track velocity. Data represent the mean \pm SEM of two independent experiments with three different fields analyzed. One-way ANOVA analysis followed by Bonferroni *post hoc* test was performed to determine significance (* $p < 0.05$, ** $p < 0.01$, *** $p < 0.001$).

Investigation. **Amets Sáenz:** Writing – review & editing, Validation, Resources, Formal analysis. **Carmen Gil:** Writing – review & editing, Supervision, Resources, Project administration, Formal analysis, Conceptualization. **Valle Palomo:** Writing – review & editing, Validation, Supervision, Formal analysis, Conceptualization. **Ángeles Martín-Requero:** Writing – review & editing, Writing – original draft, Validation, Resources, Formal analysis, Conceptualization. **Ana Martínez:** Writing – review & editing, Writing – original draft, Validation, Resources, Project administration, Funding acquisition, Formal analysis, Conceptualization.

Declaration of competing interest

The authors declare that the research was conducted in the absence of any commercial or financial relationships that could be construed as a potential conflict of interest.

Data availability

Data will be made available on request.

Acknowledgments

We are grateful to the patients, healthy volunteers and clinicians

involved in this study for providing samples. We acknowledge the support of the publication fee by the CSIC Open Access Publication Support Initiative through its Unit of Information Resources for Research (URICI). Part of the work presented on this research article was awarded the Lilly Award from the Spanish Society of Medicinal Chemistry (SEQT) and Lilly S.A on the 2023 edition.

Appendix A. Supplementary data

Supplementary data to this article can be found online at <https://doi.org/10.1016/j.nbd.2024.106430>.

References

- Alquezar, C., Salado, I.G., de la Encarnación, A., Pérez, D.I., Moreno, F., Gil, C., et al., 2016a. Targeting TDP-43 phosphorylation by casein kinase-18 inhibitors: a novel strategy for the treatment of frontotemporal dementia. *Mol. Neurodegener.* 11 (1), 36.
- Askanas, V., Engel, W.K., 1975. A new program for investigating adult human skeletal muscle grown aneurally in tissue culture. *Neurology.* 25 (1), 58–67.
- Ayers, J.I., Giasson, B.I., Borchelt, D.R., 2018. Prion-like spreading in Tauopathies. *Biol. Psychiatry* 83 (4), 337–346.
- Bayer, T.A., 2015. Proteinopathies, a core concept for understanding and ultimately treating degenerative disorders? *Eur. Neuropsychopharmacol.* 25 (5), 713–724.
- Berning, B.A., Walker, A.K., 2019. The pathobiology of TDP-43 C-terminal fragments in ALS and FTL. *Front. Neurosci.* 13, 335.

- Braak, H., Brettschneider, J., Ludolph, A.C., Lee, V.M., Trojanowski, J.Q., Del Tredici, K., 2013. Amyotrophic lateral sclerosis—a model of corticofugal axonal spread. *Nat. Rev. Neurol.* 9 (12), 708–714.
- Brettschneider, J., Del Tredici, K., Toledo, J.B., Robinson, J.L., Irwin, D.J., Grossman, M., et al., 2013. Stages of pTDP-43 pathology in amyotrophic lateral sclerosis. *Ann. Neurol.* 74 (1), 20–38.
- Brooks, B.R., Miller, R.G., Swash, M., Munsat, T.L., 2000. World Federation of Neurology Research Group on motor neuron D. El Escorial revisited: revised criteria for the diagnosis of amyotrophic lateral sclerosis. *Amyotroph. Lateral Scler. Other Motor Neuron Disord.* 1 (5), 293–299.
- Burk, K., Pasterkamp, R.J., 2019. Disrupted neuronal trafficking in amyotrophic lateral sclerosis. *Acta Neuropathol.* 137 (6), 859–877.
- Casarotto, E., Sproviero, D., Corridori, E., Gagliani, M.C., Cozzi, M., Chierichetti, M., et al., 2022. Neurodegenerative disease-associated TDP-43 fragments are extracellularly secreted with CASA complex proteins. *Cells.* 11 (3).
- Chakraborty, R., Nonaka, T., Hasegawa, M., Zurzolo, C., 2023. Tunneling nanotubes between neuronal and microglial cells allow bi-directional transfer of α -Synuclein and mitochondria. *Cell Death Dis.* 14 (5), 329.
- Cordero Cervantes, D., Zurzolo, C., 2021. Peering into tunneling nanotubes—the path forward. *EMBO J.* 40 (8), e105789.
- Cuevas, E.P., Rodríguez-Fernández, A., Palomo, V., Martínez, A., Martín-Requero, A., 2022. TDP-43 pathology and prionic behavior in human cellular models of Alzheimer's disease patients. *Biomedicines.* 10 (2), 385.
- Ding, X., Ma, M., Teng, J., Teng, R.K., Zhou, S., Yin, J., et al., 2015. Exposure to ALS-FTD-CSF generates TDP-43 aggregates in glioblastoma cells through exosomes and TNTs-like structure. *Oncotarget* 6 (27), 24178–24191.
- Hayes, L.R., Kalab, P., 2022. Emerging therapies and novel targets for TDP-43 Proteinopathy in ALS/FTD. *Neurotherapeutics.* 19 (4), 1061–1084.
- Hergesheimer, R., Lanznaster, D., Bourgeois, J., Héroult, O., Vourc'h, P., Andres, C.R., et al., 2020. Conditioned medium from cells overexpressing TDP-43 alters the metabolome of recipient cells. *Cells* 9 (10), 2198.
- Hussain, T., Mulherkar, R., 2012. Lymphoblastoid cell lines: a continuous in vitro source of cells to study carcinogen sensitivity and DNA repair. *Int J Mol Cell Med.* 1 (2), 75–87.
- Lagalwar, S., 2022. Mechanisms of tunneling nanotube-based propagation of neurodegenerative disease proteins. *Front. Mol. Neurosci.* 15, 957067.
- Liu, X., Henty-Ridilla, J.L., 2022. Multiple roles for the cytoskeleton in ALS. *Exp. Neurol.* 355, 114143.
- Martínez-González, L., Rodríguez-Cueto, C., Cabezedo, D., Bartolomé, F., Andrés-Benito, P., Ferrer, I., et al., 2020. Motor neuron preservation and decrease of in vivo TDP-43 phosphorylation by protein CK-1 δ kinase inhibitor treatment. *Sci. Rep.* 10 (1), 4449.
- Martínez-González, L., Gonzalo-Consuegra, C., Gómez-Almería, M., Porras, G., de Lago, E., Martín-Requero, Á., et al., 2021. Tideglusib, a non-ATP competitive inhibitor of GSK-3 β as a drug candidate for the treatment of amyotrophic lateral sclerosis. *Int. J. Mol. Sci.* 22 (16), 8975.
- Masrori, P., Van Damme, P., 2020. Amyotrophic lateral sclerosis: a clinical review. *Eur. J. Neurol.* 27 (10), 1918–1929.
- Mishra, P.S., Boutej, H., Soucy, G., Bareil, C., Kumar, S., Picher-Martel, V., et al., 2020. Transmission of ALS pathogenesis by the cerebrospinal fluid. *Acta Neuropathol. Commun.* 8 (1), 65.
- Neumann, M., Sampathu, D.M., Kwong, L.K., Truax, A.C., Micsenyi, M.C., Chou, T.T., et al., 2006. Ubiquitinated TDP-43 in frontotemporal lobar degeneration and amyotrophic lateral sclerosis. *Science.* 314 (5796), 130–133.
- Nozal, V., Martínez-Gonzalez, L., Gomez-Almeria, M., Gonzalo-Consuegra, C., Santana, P., Chaikuad, A., et al., 2022. TDP-43 modulation by tau-tubulin kinase 1 inhibitors: a new avenue for future amyotrophic lateral sclerosis therapy. *J. Med. Chem.* 65 (2), 1585–1607.
- Oliva, M., Tosat-Bitrián, C., Barrado-Gil, L., Bonato, F., Galindo, I., Garaigorta, U., et al., 2022. Effect of clinically used microtubule targeting drugs on viral infection and transport function. *Int. J. Mol. Sci.* 23 (7), 3448.
- Polymenidou, M., Cleveland, D.W., 2012. Prion-like spread of protein aggregates in neurodegeneration. *J. Exp. Med.* 209 (5), 889–893.
- Porras, G., Ruiz, S., Maestro, I., Borrego-Hernández, D., Redondo, A.G., Martínez, A., et al., 2023. Functional characterization of a familial ALS-associated missense TBK1 (p-Arg573Gly) mutation in patient-derived lymphoblasts. *Int. J. Mol. Sci.* 24 (3), 2847.
- Porta, S., Xu, Y., Restrepo, C.R., Kwong, L.K., Zhang, B., Brown, H.J., et al., 2018. Patient-derived frontotemporal lobar degeneration brain extracts induce formation and spreading of TDP-43 pathology in vivo. *Nat. Commun.* 9 (1), 4220.
- Posa, D., Martínez-Gonzalez, L., Bartolome, F., Nagaraj, S., Porras, G., Martínez, A., et al., 2019. Recapitulation of pathological TDP-43 features in immortalized lymphocytes from sporadic ALS patients. *Mol. Neurobiol.* 56 (4), 2424–2432.
- Salado, I.G., Redondo, M., Bello, M.L., Perez, C., Liachko, N.F., Kraemer, B.C., et al., 2014. Protein kinase CK-1 inhibitors as new potential drugs for amyotrophic lateral sclerosis. *J. Med. Chem.* 57 (6), 2755–2772.
- Soo, K.Y., Farg, M., Atkin, J.D., 2011. Molecular motor proteins and amyotrophic lateral sclerosis. *Int. J. Mol. Sci.* 12 (12), 9057–9082.
- Tamaki, Y., Ross, J.P., Alipour, P., Castonguay, C., Li, B., Catoire, H., et al., 2023. Spinal cord extracts of amyotrophic lateral sclerosis spread TDP-43 pathology in cerebral organoids. *PLoS Genet.* 19 (2), e1010606.
- Tzeplaeff, L., Wilfling, S., Requardt, M.V., Herdick, M., 2023. Current state and future directions in the therapy of ALS. *Cells.* 12 (11), 1523.
- Vaca, G., Martínez-Gonzalez, L., Fernandez, A., Rojas-Prats, E., Porras, G., Cuevas, E.P., et al., 2021. Therapeutic potential of novel cell division cycle kinase 7 inhibitors on TDP-43-related pathogenesis such as frontotemporal lobar degeneration (FTLD) and amyotrophic lateral sclerosis (ALS). *J. Neurochem.* 156 (3), 379–390.
- Vargas, J.Y., Grudina, C., Zurzolo, C., 2019. The prion-like spreading of α -synuclein: from in vitro to in vivo models of Parkinson's disease. *Ageing Res. Rev.* 50, 89–101.
- Wang, Y., Cui, J., Sun, X., Zhang, Y., 2011. Tunneling-nanotube development in astrocytes depends on p53 activation. *Cell Death Differ.* 18 (4), 732–742.
- Wilson 3rd, D.M., Cookson, M.R., Van Den Bosch, L., Zetterberg, H., Holtzman, D.M., Dewachter, I., 2023. Hallmarks of neurodegenerative diseases. *Cell* 186 (4), 693–714.